Research Article

Yating Mao, Mingyang Tan, Tia C. L. Kohs, Joanna L. Sylman, Anh T. P. Ngo, Cristina Puy, Owen J. T. McCarty, and Travis W. Walker*

Transient particle tracking microrheology of plasma coagulation via the intrinsic pathway

https://doi.org/10.1515/arh-2022-0129
received February 28, 2022; accepted October 04, 2022

Abstract: The maintenance of hemostasis to ensure vascular integrity is dependent upon the rapid conversion of zymogen species of the coagulation cascade to their enzymatically active forms. This process culminates in the generation of the serine protease thrombin and polymerization of fibrin to prevent vascular leak at sites of endothelial cell injury or loss of cellular junctions. Thrombin generation can be initiated by the extrinsic pathway of coagulation through exposure of blood to tissue factor at sites of vascular damage, or alternatively by the coagulation factor (F) XII activated by foreign surfaces with negative charges, such as glass, through the contact activation pathway. Here, we used transient particle tracking microrheology to investigate the mechanical properties of fibrin in response to thrombin generation downstream of both coagulation pathways. We found that the structural heterogeneity of fibrin formation was dependent on the reaction kinetics of thrombin generation. Pharmacological inhibition of FXII activity prolonged the time to form fibrin and increased the degree of heterogeneity of fibrin, resulting in fibrin clots with reduced mechanical properties. Taken together, this study demonstrates a dependency of the physical biology of fibrin formation on activation of the contact pathway of coagulation.

Keywords: microrheology, coagulation, heterogeneity

□□
* Corresponding author: Travis W. Walker, Chemical and Biological Engineering, South Dakota School of Mines & Technology, Rapid City, SD, USA, e-mail: travis.walker@sdsmt.edu
Yating Mao: Department of Chemical and Biomedical Engineering, FAMU-FSU College of Engineering, FLorida State University, Tallahassee, FL, USA
Mingyang Tan: Institute of Materials Science, University of Connecticut, Storrs, CT, USA
Tia C. L. Kohs, Joanna L. Sylman, Anh T. P. Ngo, Cristina Puy, Owen J. T. McCarty: Biomedical Engineering, School of Medicine, ORegon Health and Science University, Portland, OR, USA

1 Introduction

The activation of the blood coagulation system is triggered by the exposure of blood to tissue factor (TF) at sites of vascular injury or the activation by foreign surfaces of the contact activation pathway [1] (Figure 1). TF initiates the activation of the extrinsic pathway of blood coagulation by converting the zymogen factor (F) VII to the active enzyme species FVIIa [2]. Charged surfaces including components of biomaterials or bacterial-derived long-chain polyphosphates (LCPPs) that initiate blood coagulation by activating coagulation FXII to FXIIa, which in turn activates FXI to lead to activation of FIX [3]. Both the extrinsic and contact activation pathways converge on the common pathway of coagulation by activating FX, which results in the generation of thrombin. Beyond activating blood cells including platelets, thrombin cleaves fibrinogen to fibrin, which polymerizes to form a fibrin mesh as part of a hemostatic plug, or a cloak to isolate bacteria or biomaterials from the blood microenvironment [1,3]. In diseases such as thrombosis, the rate of thrombin generation outpaces the rate of inactivation of the serine proteases of the coagulation cascade, resulting in occult intravascular thrombosis formation underlying pathologies including myocardial infarction, pulmonary embolism, and disseminated intravascular coagulopathy [4,5].

The conversion of fibrinogen from a soluble form to a meshwork of polymerized fibrin has been shown to be dependent upon both the pathway of initiation and the rate of thrombin generation. These variables have been shown to regulate the physical biology of fibrin, including individual fiber length and diameter as well as bulk cross-linking and tertiary structures, all of which affect clot strength and resistance to breakdown [6,7]. However, the majority of these mechanistic studies have been performed under static conditions; as such, it has remained unclear how these pathways regulate fibrin formation in the context of the rheological environment of the circulation.

Particle tracking microrheology (PTM) is a passive microrheological technique that characterizes the microenvironment

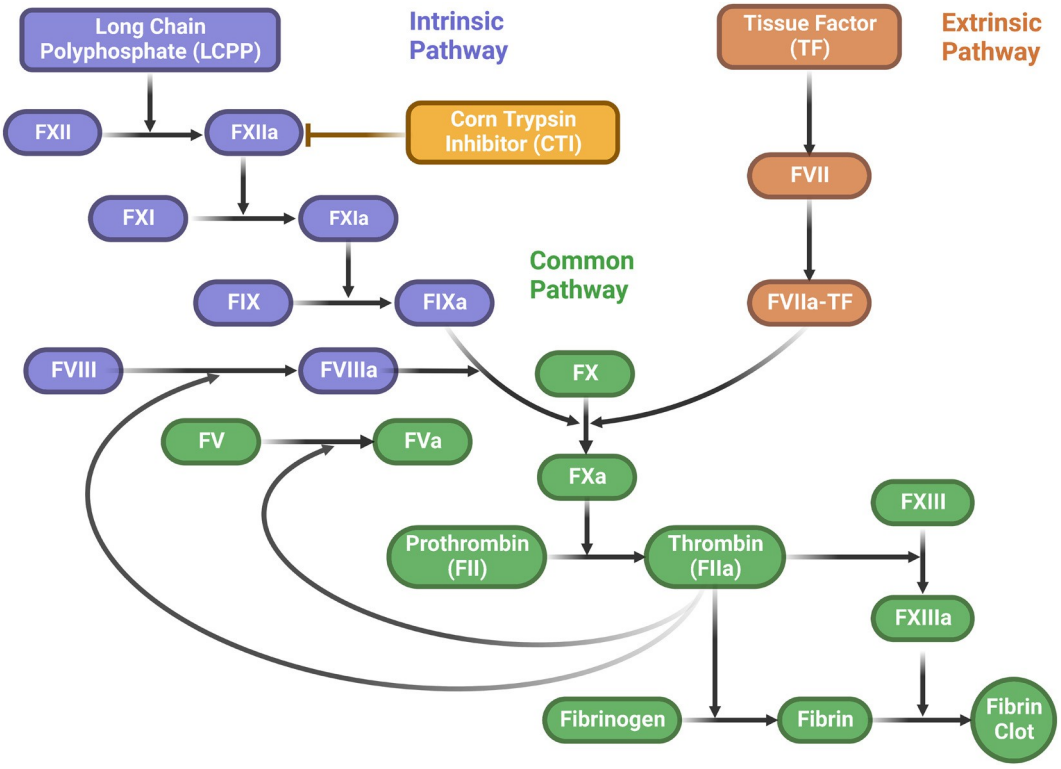

Figure 1: Schematic of the blood coagulation cascade. Activation of the coagulation cascade triggers the conversion of the inactive coagulation factors (represented by an F followed by a Roman number, e.g., FXII) to their active form (FXIIa) by a series of enzymatic reactions. The intrinsic pathway (purple) is also termed the "contact activation pathway," which is activated by negatively charged surfaces, such as polyphosphates. The extrinsic pathway (orange) is initiated by TF that is released during vascular injury. The activation of platelets upon injury is not depicted here. The activation of coagulation factor ten (FX) marks the start of the common pathway (green) that leads to the formation of cross-linked fibrin clots.

of a medium by tracking the Brownian motion of embedded probes. Since the driving force of Brownian motion is thermal energy, these particles perturb the fibrin filaments by minimal deformations, ensuring that the internal structure of the fibrin clots remains intact throughout the transient process of coagulation [8,9].Thus, this platform represents a useful and sensitive method to evaluate the effect of initiation of the coagulation cascade downstream the TF pathway as compared to the contact pathway of coagulation on the mechanics and dynamics of fibrin formation. In this investigation, platelet poor plasma (PPP) excluding platelet activities was used to form fibrin clots. Calcium participates in a series of enzymatic reactions and fibrin polymerization, thus calcium chloride was added to all clotting samples. Vehicle control group includes samples treated with the same solvent as for the test groups. After the fibrin clots equilibrated, we used scanning confocal microscopy to visualize the network of the clots. A statistical heterogeneity analysis proposed by Valentine et al. [10] was adopted in the microrheological measurements. The results suggested different levels of heterogeneity in the fibrin clots, where the wide distribution of the diffusive exponents in the LCPP/corn trypsin inhibitor (CTI) group indicated the most heterogeneous structure. Quantitative analysis of the confocal images showed that LCPP and LCPP/CTI samples had the shortest fibrin filaments, ~ 7.75 and $\sim 8.85\ \mu m$, respectively.

2 Materials and methods

Poly(ethylene glycol) (PEG)-ylated particles were prepared by coupling the carboxylate-modified fluorescent probing particles (Molecular Probes, FluoSpheres, $1\ \mu m$ yellow-green (505/515)) with methoxy-PEG-amine (Layson Bio, 5,000 Da), using 1-ethyl-3-(3-dimethylaminopropyl) carbodiimide (ThermoFisher), N-hydroxysuccinimide (Sigma-Aldrich), and 2-(N-morpholino)ethane sulfonic acid (Sigma-Aldrich) [11,12]. PPP was purchased from Innovative Research. LCPP (1,000 phosphate units) and biotinylated polyphosphate (200–1,300 phosphate units) were kind gifts from Stephanie Smith and Jim Morrissey and prepared following the

procedures that were outlined by Morrissey and co-workers [13,14]. CTI was purchased from Haemotologic Technologies. Lipidated recombinant TF was purchased from Siemens, Dade Innovin reagent. 4-(2-Hydroxyethyl)-1-piperazineethanesulfonic acid (HEPES)-buffered saline contained 25 mM of HEPES (Sigma-Aldrich) and 150 mM NaCl.

2.1 Fibrin formation

Plasma coagulation was measured in flat 18-well slides (ibidi, μ-Slide 18 Well-Flat) using $30\ \mu m$ of plasma in single reservoirs. In selected experiments, the plasma samples were pretreated with CTI (40 g/mL), which binds and inactivates the activated FXIIa. The activation is achieved by incubation of plasma with LCPP (100 mM). Alternatively, the extrinsic pathway of coagulation was initiated by incubation of plasma with TF (0.01 nM). HEPES-buffered saline served as the diluent. The coagulation of all samples was initiated with 13.7 mM $CaCl_2$. The vehicle control group includes samples tested with the same solvents as for the test groups, which is composed of HEPES (25 mM)-buffered saline (150 mM NaCl) and 13.7 mM $CaCl_2$. Following the sonication that ensures the monodispersity of fluorescent particles, $1\ \mu m$ of them were added with $CaCl_2$ at a volume fraction of 1.3×10^{-5}. All concentrations listed are the final concentrations in the plasma solutions.

2.2 Theory of microrheology

In a passive microrheology experiment, the mean-squared displacement (MSD) of submicron- to micron-scale probing particles that are embedded in the material of interest are measured [15]. The measurements are achieved by tracking the probes' Brownian motions, which are driven by the thermal energy that induces minimal local deformations to the medium. For particles with comparable size to the intrinsic mesh size of the material, the thermal fluctuations of these particles reflect the microscopic environment of the material. Particles that are much smaller than the mesh size will diffuse through the interstitial fluid as if they reside in a Newtonian fluid. Particles that are much larger than the mesh size will probe the material over a large averaged area, providing essentially a bulk description of the material.

In a Newtonian fluid, the MSD of the probing particles increases with time, such that

$$\langle\langle \Delta r^2(\tau)\rangle_\tau \rangle = 2d D\tau, \quad (1)$$

where Δr^2 is the squared displacement, τ is the lag time, $\langle \cdot \rangle_\tau$ indicates the time average, $\langle \cdot \rangle$ indicates the ensemble average, d is the dimensionality of the tracked motion, and D is the diffusivity of the particle. For the particles that reside in a Hookean solid, the MSD remains constant over time. The MSDs of viscoelastic materials have been found to empirically follow a power-law relation with the lag time [16,17], such that

$$\langle\langle \Delta r^2(\tau)\rangle_\tau \rangle = \left\langle \Delta r^2\left(\frac{1}{\omega_0}\right)\right\rangle (\omega_0\tau)^{\alpha(\omega_0)}, \quad (2)$$

where $\langle \Delta r^2(1/\omega_0)\rangle$ is the MSD at $\tau = 1/\omega_0$, and α is the power law exponent ($0 \le \alpha \le 1$). Here, ω_0 represents the frequency at which the rheological properties are being determined, and this frequency can be subsequently varied in the analysis. Thus, α is also the logarithmic slope of the MSD at $\tau = 1/\omega_0$ [18]. The logarithmic slope is unity for Newtonian fluids and zero for Hookean solids. For viscoelastic materials that behave somewhere between a pure solid and a pure liquid, the slope ranges between zero and one. Thus α is also called the diffusive exponent, which indicates the viscoelastic response of the medium when it is probed by the particles. The MSD of microscopic probes has been quantitatively related to the complex shear moduli, G^*, that are used to characterize complex fluids in macroscopic rheology by Mason et al. [16,18], such that

$$G^*(\omega_0) = \frac{dk_BT\ \exp\left(\frac{i\pi\alpha}{2}\right)}{3\pi a\langle \Delta r^2(\omega_0)\rangle \Gamma[1+\alpha(\omega_0)]}, \quad (3)$$

where Γ is the gamma function. The elastic (G') and the viscous (G'') shear moduli can be further computed by applying Euler's equation. The validity of the generalized Stokes–Einstein relation (GSER, equation (3)) is highly dependent on its assumptions [16,17]. Discussions of the violation and break down of the GSER can be found in previous studies [17,19].

2.3 Video microscopy

The Brownian motion of the probing particles was recorded at a frame rate of 31 fps by a video microscopy system, which includes an inverted fluorescent microscope (Nikon, Ti-S), a charged-couple device camera (Allied Vision, Guppy Pro 125B), a light-emitting diode (LED) light source (X-cite, 120LED), and a computer that was used for image acquisition

and data analysis. A 40×/0.6 NA air immersion objective (Nikon) was employed for imaging the particles. Video recordings were started after 2 min of loading and sealing of the initiated PPP solution. The motions of probing particles were recorded throughout the development of the fibrin network from its initial state as a purely viscous liquid to its presumed final state as an elastic solid.

2.4 Image analysis

The MSD was obtained by locating the positions of the probing particles in consecutive images that were acquired by the microscopy setup, utilizing a MATLAB tracking algorithm that was adapted from the five-step routines originally developed by Crocker and Grier in IDL [20]. Static and dynamic errors have been identified in previous work by the authors for the same system [21]. These errors were corrected during the data analysis by following the method in the study by Savin and Doyle [22].

We applied the PTM to measure the transient microrheology of the evolving fibrin clots. We characterized coagulation by the gelation time and the quality of the clot at the gel point, which can be characterized by the shear moduli of the clot at this characteristic time. The transition of a material from liquid state to solid state can be described by the gradual decrease in the slope of the MSD of the embedded probing particles. To study the properties of the plasma at different stages through the process of coagulation, we divided each of the videos into 30 segments and computed the MSD of the first 1/10 of the frames of the duration of each segment to ensure that the sample was at a quasi-equilibrium state during the measurement. However, noticeable convection, which causes the diffusive exponent to be greater than unity, was observed in the first few minutes of the gelation, which was attributed to the sealing step of the sample preparation. Therefore, in all of the plots of transitioning MSD and in plots of the value of α that are shown below, data are plotted from the point that the sample starts to show a stable transition.

2.5 Confocal microscopy

Confocal images were taken by a laser scanning confocal microscope (Leica, DMI 4000B) with a 40 ×/1.15 NA oil immersion objective (Leica) and an excitation laser at the wavelength of 488 nm. The confocal microscope is controlled by the Leica application suite for Advanced Fluorescence. The confocal images of equilibrated fibrin clots were taken 24 h after the microrheological measurements. Image processing was completed in MATLAB. Quantification of the fibrin filaments in the confocal images was performed using ImageJ. The filament lengths were manually measured using the “straight line” and “segment line” tool. All filaments presented in each confocal image were selected for the measurements, and the “number of measurements” shown in Table 1 reflects the number of measured filaments. To measure the “filament coverage” in ImageJ, a threshold was applied to each image with a white background; then the circular shapes were selected and color-inverted to have the same color as the background; finally, the “filament coverage” area was obtained by using the “analyze particles” function.

3 Results and discussion

3.1 Interpreting MSDs

Examples of transient MSDs of evolving fibrin clots are shown in Figure 2. The experiment in Figure 2(a) was initiated with vehicle control with no inhibitor, while the experiment in Figure 2(c) was initiated by LCPP to incite FXII activation and coagulation by the contact pathway; in selected experiments, activated FXIIa was inhibited by CTI. These samples were chosen specifically to visualize the differences in the spatial evolution of the fibrin clots when thrombin generation is initiated by the contact pathway. The slope values of the MSDs are plotted as a function of time for these two samples in

Table 1: Quantitative analysis of the fibrin filaments corresponding to each confocal image in Figure 6

	Vehicle	TF	LCPP	CTI	TF/CTI	LCPP/CTI
Average length (μm)	12.868	32.811	7.746	17.089	13.199	8.582
Minimum length (μm)	3.574	7.522	1.349	6.711	2.645	1.833
Maximum length (μm)	54.051	77.03	40.09	35.529	51.948	57.705
Standard deviation (μm)	7.011	16.313	5.028	5.946	7.449	6.074
Number of measurements	222	49	246	93	142	195
Filament coverage (%)	16.569	12.841	11.861	14.266	11.499	7.526

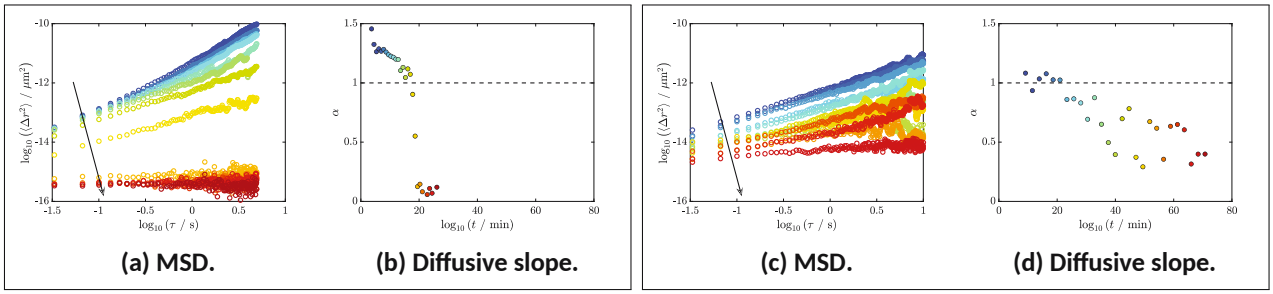

Figure 2: Ensemble-averaged MSDs of fibrin clots throughout the polymerization versus time. (a)–(b) Vehicle. (a) The MSD of an evolving fibrin clot that was initiated with vehicle control. The slope of MSD decreased as fibrin cross-linked, as indicated by the downward arrow. This decrease is also color-coded by the transition from blue (early stage) to red (late stage). (b) The logarithmic slopes of each MSD as in (a). The same color codes are used here as in (a). A dashed line with the value of one is given here in reference to the diffusion of a Newtonian fluid. (c) and (d) LCPP and CTI. (c) The MSD of an evolving fibrin clot that was initiated by LCPP and inhibited by CTI. The downward arrow suggests the decrease in MSD over time. This decrease is also marked by the color gradient from blue to red. (d) The logarithmic slopes of each MSD as in (c). The same color codes are used here as in (c). Some time segments of MSD in (a) and (c) were removed for a clearer view of the transition of the MSD over time, but all values of α are reported in (b) and (d). A dashed line with the value of one is given here in reference to the diffusion of a Newtonian fluid.

Figure 2(b) and (d), respectively. For both samples, the initial MSD has a slope of approximately one, which indicates that the PPP solution was initially a Newtonian fluid. The MSD gradually decreased over time as the fibrin polymerized, showing increasing elasticity of the clot.

Detailed information about the mechanical properties during the evolution of the clot can be further extracted from these transient plots. For instance, the last MSD of Figure 2(a) is smaller in area and closer to zero than the final MSD of Figure 2(c) over the same time. We predict that if the experiment was allowed to progress, the samples containing both LCPP and CTI may eventually show a constant MSD; regardless, these results indicate that relative to the vehicle control baseline, a reduction in rigidity reflected by an increase in the mobility of probe particles was observed when fibrin formation incited by LCPP in the presence of the FXIIa inhibitor CTI. Moreover, compared to the sample with the addition of LCPP and CTI, the slopes of the sample under vehicle control show a cleaner transition. This observation indicates that a more heterogeneous structure is being formed when LCPP and CTI are added, as fibrin clots are not formed throughout the entire medium, but they are instead more localized. Thus, particles experience different local structures, which are revealed by a fluctuation of diffusive exponents α. Although LCPP initiates the intrinsic pathway by activating FXII and by serving as a cofactor of FIX and prothrombin (FII), bypassing the activation of FXI [23], FXIIa as well as FXI can be inhibited by CTI at a 1:1 stoichiometry. Therefore, with the presence of CTI, LCPP may only serve as the cofactor of FIX and FII, resulting in the formation of a fibrin clot with lower rigidity.

3.2 Heterogeneity of fibrin clots

Experiments were run until the particles were considered motionless. We found that the last overall MSD of the gelation, which is an ensemble average of all available

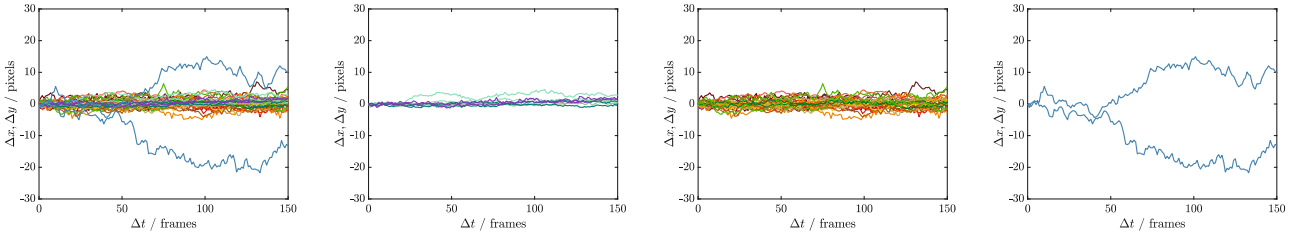

Figure 3: Displacement in x- and y-directions of independent particles that were presented in the first 150 frames in the 36th min of the coagulation of PPP with LCPP and CTI. The same color indicates the displacement in two directions of the same particle. (a) Displacement of all particles in this time frame. Most particles have small displacements, but one particle is very mobile. (b) Displacement of particles in Group I. These highly confined particles showed very low displacements. (c) Displacement of particles in Group II. These particles are less confined, showing slightly larger displacements than Group I. (d) Displacement of a single particle in Group III. Instead of being constrained, this particle was quite diffusive, as it was able to presumably travel more freely in the interstitial spaces of the material.

particles, did not always decrease to a constant value as expected based on these observations. Therefore, we investigated the displacement of single particles in different segments. For example, Figure 3(a) shows the displacement of particles in both x- and y-directions that were presented in the first 150 frames of the 36th min of the coagulation of plasma with LCPP and CTI, where the inconsistent displacements of single particles are easily distinguishable. After applying a variance test (F-test [10,24]) to the displacements of each particle in both directions, particles were categorized into groups on the basis of their differences in the variances of displacements. Only one group of motion will be found in a homogeneous medium, but multiple groups can exist in a heterogeneous material, depending on the level of heterogeneity of the microscopic structure. For this example experiment, three groups were found (Figure 3(b)–(d)). The particles in Group I (Figure 3(b)) were highly confined by the cross-linked network. The particles in Group II (Figure 3(c)) were less confined. When compared to the particles in these two groups, Groups I and II, one particle, shown in Group III, were very mobile (Figure 3(d)). The displacement of this diffusive particle contributes to a significant increase in the ensemble-averaged MSD of the system. The motion of early entrapped particles can also induce a substantial decrease in the ensemble-averaged MSD.

Regardless of the time (e.g., the 36th minute in the previous example) that a sample is analyzed, inconsistencies in the displacements of different particles were found in all samples in this study to various extents. This variant motion of single particles signifies a heterogeneous structure of the fibrin clots. Thus, we replotted the values of the diffusive exponents that were based on the groupings, as shown in Figure 4. Here, α_{mode} is the slope of the ensemble-averaged MSD of the group with the largest population, and α_{max} and α_{min} are slopes of the groups with the maximum and minimum value of α, respectively. Note that a homogeneous sample should contain one group such that $\alpha_{\mathrm{mode}} = \alpha_{\mathrm{max}} = \alpha_{\mathrm{min}}$. From Figure 4, the diffusive exponents of all groups basically

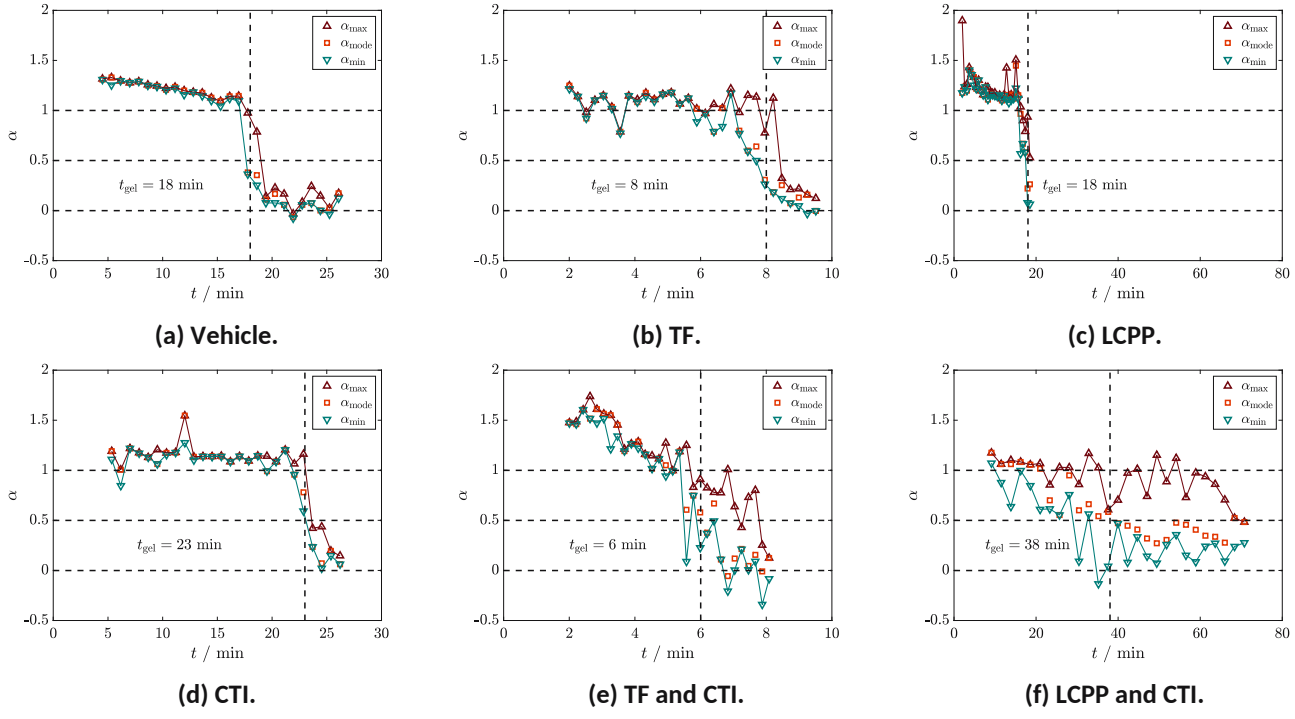

Figure 4: Representative examples for all reaction conditions. The values of the diffusive exponent α, that were grouped on the basis of the mobility of the particles. The variable α_{mode} is the slope of the MSD of the group with the most particles, while α_{min} and α_{max} are the values of α for the groups with the lowest and highest slope value in the specific time of analysis. (a) Fibrin clot that was formed with vehicle control. This result showed a low level of heterogeneity in the sol–gel transitioning region. (b) Evolving fibrin clot that was initiated by TF. This clot developed a heterogeneous sol–gel transitioning region. (c) Fibrin clot was formed with LCPP. This sample showed a relatively low level of heterogeneity. (d) Fibrin clot was formed with the inhibition by CTI. The heterogeneity was mainly developed in the transitioning region. (e) Fibrin clot was formed with TF and inhibited by CTI. The heterogeneity was also developed in the transitioning region. (f) Fibrin clot was initiated by LCPP and inhibited by CTI. This clot exhibited the highest heterogeneity, which was observed throughout the coagulation.

overlap in the early stages of thrombin generation and fibrin formation, as all particles still reside in one group. As the reaction progressed, spatially dependent reaction kinetics produced heterogeneity in the sample, which caused a spread in the values of α in the transitioning region. Different levels of heterogeneity can be seen in different samples, as shown in Figure 4. Figure 4(f) exhibits the highest heterogeneity, which we assume is caused by the inhibition of FXIIa by CTI, as discussed previously. In Figure 4(f), the maximum and minimum values of α are very distinguishable, which reflects the motion of both diffusive particles and constrained particles in the system. However, the motions of the majority of the particles (α_{mode}) show a relatively clean transition, which is considered to be more representative of the gelation.

3.3 Gel point

A developing clot is a dynamic system that results in a weak hydrogel. During the gelation the sample progresses through states of being a viscoelastic liquid before the gel point and a viscoelastic solid after the gel point. Eventually, the sample is so rigid that it could be considered a purely elastic Hookean solid. One method to find the gel point is by observing how the moduli develop over time for a wide range of frequencies using the theory of time-cure superposition [25–27]. However, the rapid polymerization of fibrin only allows for short times of analysis, and the relaxation time is not accessible in this small range of frequencies.

Alternatively, the Rouse prediction of $G(t) \sim t^{-1/2}$ has been successfully used to identify the critical gel point of gelling systems [25,28–30]. At the gel point t_{gel}, the elastic (solid-like) storage modulus, G', and the viscous (liquid-like) loss modulus, G'', crossover such that G' will dominate. In microrheology, the Rouse prediction of the gel point can be adjusted to $\langle \Delta r^2(t) \rangle \sim t^{1/2}$. Therefore, we used $\alpha_{\text{mode}} = 1/2$ as the criterion to identify the gel point t_{gel}.

The gel points of all samples that were measured are shown in Figure 5(a). The reaction kinetics of the samples that were initiated by TF (extrinsic pathway) do not appear to be significantly affected by the inhibition by CTI. This result is reasonable, as TF is an initiator of the extrinsic pathway, which should be indirectly affected by inhibition of FXIIa. The kinetics of thrombin generation leading to fibrin formation under vehicle control was slightly prolonged by CTI. However, CTI significantly prolonged the coagulation when LCPP was present. CTI is an inhibitor in the intrinsic pathway, and as such the effect of CTI on fibrin generated by the FXII-activating agent LCPP was directly impacted as expected.

3.4 Shear moduli at the gel point

To assess the effect of CTI introduced on the microscopic structure of clotting systems, we measured the moduli of

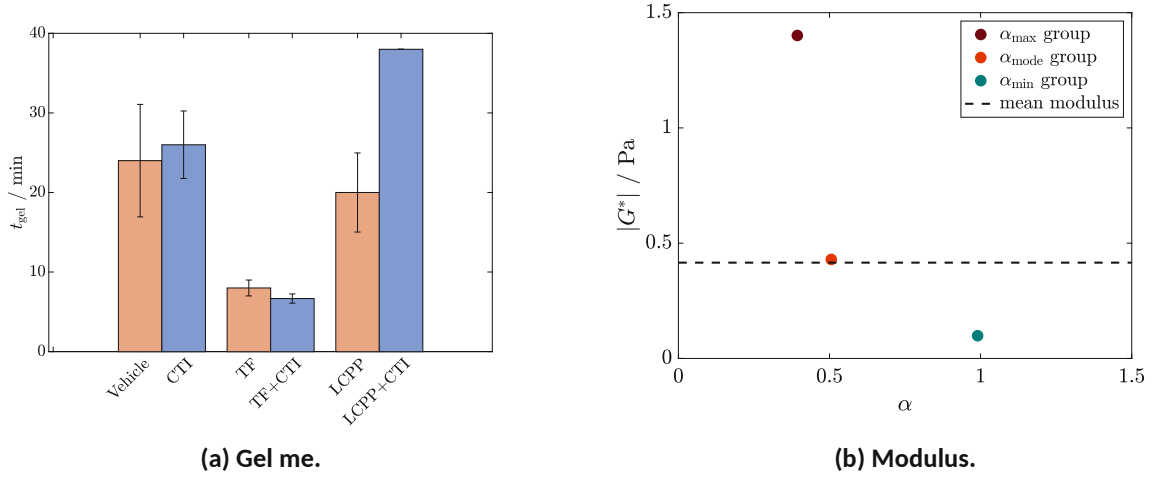

(a) Gel me. **(b) Modulus.**

Figure 5: Rheological characteristics. (a) Gel time of all samples. The error bars indicate the standard deviation of $n \in [1, 4]$ runs of each type of clot. The gel time of the clot that was initiated by LCPP was noticeably prolonged by the inhibition of CTI. (b) Example moduli (31 Hz) at the gel time of a fibrin clot that was formed with LCPP and CTI as a function of the diffusive exponent of each group of probing particles. Heterogeneous structure caused distinctive motions of probing particles, resulting in multiple moduli that reflect the local environment of each group (α_{max}, α_{mode}, and α_{min}). Less diffusive particles (with low α value) are positioned in denser networks (with high $|G^*|$), and vice versa. $\langle |G^*| \rangle$ is determined using the ensemble-averaged MSD of all probes in the field of view.

these clots at their gel point by applying equation (3). At a chosen time, the value of the moduli is determined by the value of α and the amplitude of MSD at a certain frequency. We again found heterogeneity at the gel point of the majority of all samples, resulting in multiple values of moduli at the gel time. As discussed previously, the difference in local environment caused each group of particles to show a distinctive diffusive exponent. As an example, Figure 5(b) shows the three moduli of a fibrin clot at the frequency of 31 Hz as a function of the diffusive exponent, α, at the gel time. As the local structure of the fibrin clots developed in different rates, the heterogeneity of the fibrin network contributed to the distinctive thermal fluctuations of particles in various locations. Therefore, the motion of each group of probing particles reflects the moduli of their surroundings. The moduli of the group with the most particles (Group 2) dominates among all the groups, which is shown in the similarity of the modulus of Group 2 and the modulus of the bulk $\langle|G^*|\rangle$, which is obtained from the ensemble-average of all particles. Lower values of α indicate a less diffusive environment, which is caused by denser local structure, and vice versa. Therefore, ideally, $|G^*|$ should decrease as α increases. Figure 5(b) is highly representative of this relation.

3.5 Confocal microscopy

The heterogeneous microstructure of the fibrin clots (linear structures in Figure 6) was visually confirmed by their confocal images. These confocal images were taken from the equilibrated clots at 24 h after the microrheological measurements. The particles in the confocal images include fluorescent particles and proteins or other substances (dark spots in the images) that naturally exist in plasma. The lengths and area of fibrin filaments in each figure were analyzed using ImageJ and reported in Table 1, where the “filament coverage” is the total percentage of area covered by fibrin filaments. All the blobs in the images were excluded during this area analysis. It was challenging to quantify fiber thickness. The filament coverage results suggest that all

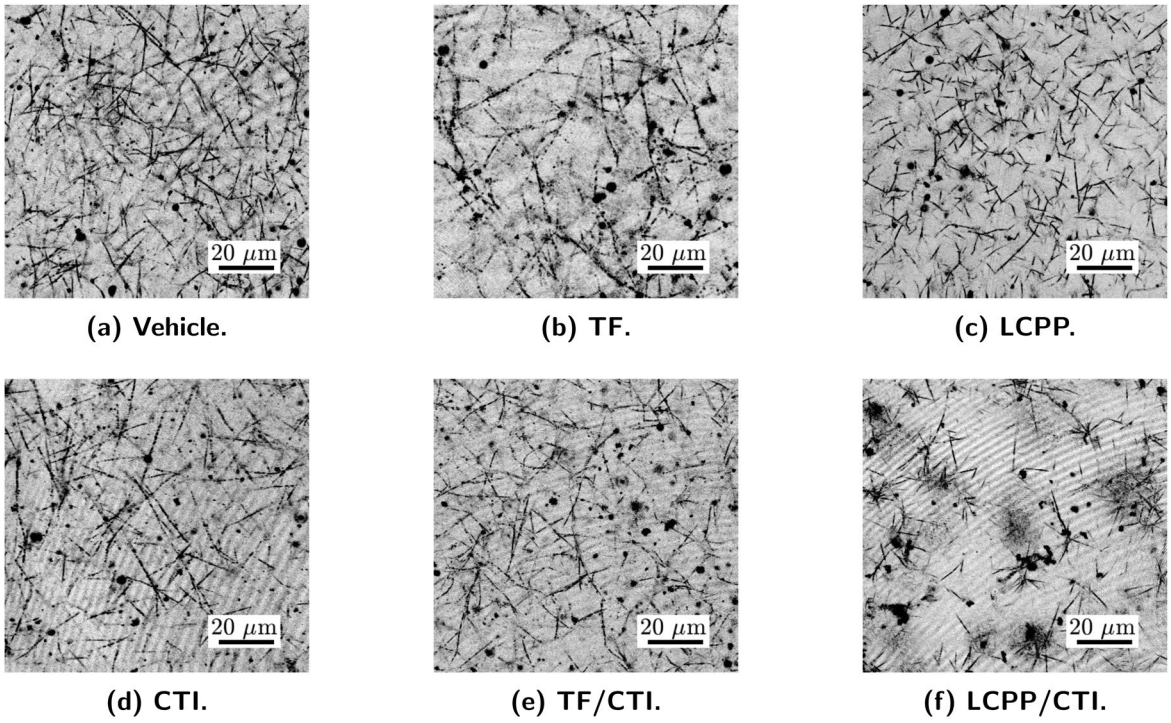

(a) Vehicle. (b) TF. (c) LCPP.

(d) CTI. (e) TF/CTI. (f) LCPP/CTI.

Figure 6: Confocal microscopy images of fibrin networks after 24 h of coagulation. The particles that are presented in the images include the probing particles as well as other substances that naturally exist in plasma. (a) A fibrin clot that was formed with vehicle control. (b) A fibrin clot that was formed with the initiation of TF, resulting in a denser network with longer fibers, compared with other samples. (c) A fibrin network that was initiated by LCPP, which also shows a dense structure. (d) A fibrin clot that was formed with the inhibition by CTI. The image shows thinner polymer fibers when compared with the vehicle-controlled sample in (a). (e) A fibrin clot that was initiated by TF with the inhibition by CTI. This clot developed thinner fibers, even though CTI and TF directly function in different pathways. (f) A fibrin clot that was initiated by LCPP and inhibited by CTI. The clotting was inhibited by CTI, resulting in a poorly developed gel with a heterogeneous structure and large voids.

samples without the addition of CTI (Figure 6(a)–(c)) formed denser fibrin networks, when correspondingly compared with the clots formed with the presence of CTI (Figure 6(d)–(f)). As shown in Table 1, the samples wherein thrombin generation and fibrin formation were initiated by TF had the longest average filament length, while the LCPP and LCPP/CTI samples had the shortest average length and standard deviations close to their average lengths. In addition, Figure 6(f) exhibits a very distinct scattered structure, which supports the observation that the development of the fibrin networks is sensitive to inhibition of FXIIa with CTI. These heterogeneous structures also explain the variant behavior of the probing particles – particles that were trapped in the structure exhibited sub-diffusive behavior, but other particles were able to travel in the voids of this network and thus show more diffusive motions.

4 Conclusion

The transition of all samples of PPP solution from a purely viscous liquid to a viscoelastic or elastic solid has been observed from the MSD as a function of time. The MSD of the original PPP solution had a diffusive exponent of one, while the diffusive exponent gradually decreased over time as the microscopic structure developed. Different levels of heterogeneity of the fibrin clots have been observed, exhibited in the deviation of diffusive exponents, α, of single particles, which indicates that the motions of the probing particles decreased at various rates. The fibrin clot that was formed with LCPP and CTI exhibited the highest deviation of α, and it also showed the highest heterogeneity in the microscopic structure that was imaged by confocal microscopy. Furthermore, the gel time, t_{gel}, of the clots that were formed with LCPP and CTI was noticeably prolonged. The addition of CTI in the PPP simulates an environment with inhibited FXIIa. Thus, FXIIa inhibition can lead to prolonged clotting time and low clot quality, which supports the hypothesis of using a targeted FXII inhibitor to suppress pathologic coagulation via the intrinsic pathway [31,32].

Our preliminary tests showed that CTI caused the fibrin clots to form with low rigidities. However, computing the bulk moduli was challenging during gelling at the micron level, since heterogeneity was seen throughout the coagulation for all trials (Figures 3 and 5(b)). To assess how the shear moduli of the fibrin clots are affected by the initiators and inhibitors, a study of the equilibrated fibrin clots should be conducted, which requires a system that prevents evaporation of any kind. Moreover, to thoroughly study the roles of FXII and FXI, a more comprehensive study of the reaction kinetics of the intrinsic pathway with a larger number of trials is necessary. Also, longer durations of experiments or multiple times of monitoring of the clotting are also necessary to identify the point that the fibrin clots start to equilibrate. Furthermore, conventional rheology of the coagulation of fibrin can provide references for the microrheological study.

Acknowledgements: The authors gratefully thank Bo Sun and Jihan Kim for the support of the confocal microscopy in this research. We thank Stephanie Smith and Jim Morrissey for the kind gift of long-chain polyphosphates.

Funding Information: This material is based upon work that was supported by the National Science Foundation under Grant Nos. 1652958 and 1842580 and the National Institute of Health Grant HL101972.

Author contributions: Yating Mao: methodology, investigation, formal analysis, visualization, writing – original draft. Mingyang Tan: methodology, formal analysis, visualization, writing – review and editing. Tia C.L. Kohs: resources, writing – review and editing. Joanna L. Sylman: resources, writing – review and editing. Anh T.P. Ngo: resources, writing – review and editing. Cristina Puy: resources, writing – review and editing. Owen T.J. McCarty: conceptualization, resources, writing – review and editing. Travis W. Walker: conceptualization, methodology, funding acquisition, supervision, writing – review and editing.

Conflict of interest: The authors hereby certify that no involvement exists of any commercial relationships or financial interests on the subject matter or materials that are discussed in the manuscript.

Ethical approval: The conducted research is not related to either human or animals use.

Data availability statement: The datasets that were generated and/or analyzed during the current study are available from the corresponding author on reasonable request.

References

[1] Smith SA, Travers RJ, Morrissey JH. How it all starts: Initiation of the clotting cascade. Critical Rev Biochem Molecular Biol. 2015;50(4):326–36.

[2] Mackman N. The role of tissue factor and factor VIIa in hemostasis. Anesthesia Analgesia. 2009;108(5):1447.
[3] Stavrou E, Schmaier AH. Factor XII: what does it contribute to our understanding of the physiology and pathophysiology of hemostasis & thrombosis. Thrombosis Res. 2010;125(3):210–5.
[4] Papageorgiou C, Jourdi G, Adjambri E, Walborn A, Patel P, Fareed J, et al. Disseminated intravascular coagulation: an update on pathogenesis, diagnosis, and therapeutic strategies. Clin Appl Thrombosis/Hemostasis. 2018;24(suppl 9):8S–28S.
[5] Mann KG, Butenas S, Brummel K. The dynamics of thrombin formation. Arteriosclerosis Thrombosis Vascular Biol. 2003;23(1):17–25.
[6] Kattula S, Byrnes JR, Wolberg AS. Fibrinogen and fibrin in hemostasis and thrombosis. Arteriosclerosis Thrombosis Vascular Biol. 2017;37(3):e13–21.
[7] Weisel JW, Litvinov RI. Fibrin formation, structure and properties. Fibrous Proteins Struct Mech. 2017;82:405–56.
[8] Mao Y, Nielsen P, Ali J. Passive and active microrheology for biomedical systems. Front Bioeng Biotechnol. 2022;10:916354.
[9] Wirtz D. Particle-tracking microrheology of living cells: principles and applications. Ann Rev Biophys. 2009;38(1):301–26.
[10] Valentine MT, Kaplan PD, Thota D, Crocker JC, Gisler T, Prud'homme RK, et al. Investigating the microenvironments of inhomogeneous soft materials with multiple particle tracking. Phys Rev E. 2001;64(6):061506.
[11] Hermanson GT. Bioconjugate techniques. London, UK: Academic Press; 2013.
[12] Valentine M, Perlman Z, Gardel M, Shin J, Matsudaira P, Mitchison T, et al. Colloid surface chemistry critically affects multiple particle tracking measurements of biomaterials. Biophys J. 2004;86(6):4004–14.
[13] Choi SH, Collins JN, Smith SA, Davis-Harrison RL, Rienstra CM, Morrissey JH. Phosphoramidate end labeling of inorganic polyphosphates: facile manipulation of polyphosphate for investigating and modulating its biological activities. Biochemistry. 2010;49(45):9935–41.
[14] Smith SA, Choi SH, Davis-Harrison R, Huyck J, Boettcher J, Rienstra CM, et al. Polyphosphate exerts differential effects on blood clotting, depending on polymer size. Blood. 2010;116(20):4353–9.
[15] Einstein A. On the motion of small particles suspended in liquids at rest required by the molecular-kinetic theory of heat. Annalen der Physik. 1905;17:549–60.
[16] Mason TG. Estimating the viscoelastic moduli of complex fluids using the generalized Stokes-Einstein equation. Rheologica Acta. 2000;39(4):371–8.
[17] Furst EM, Squries TM. Microrheology. New York, USA: Oxford University Press; 2017.
[18] Mason TG, Weitz D. Optical measurements of frequency-dependent linear viscoelastic moduli of complex fluids. Phys Rev Lett. 1995;74(7):1250.
[19] Squires TM, Mason TG. Fluid mechanics of microrheology. Ann Rev Fluid Mechanics. 2010;42:413–38.
[20] Crocker JC, Grier DG. Methods of digital video microscopy for colloidal studies. J Colloid Interface Sci. 1996;179:298–310.
[21] Tan M, Mao Y, Walker TW. Rheological enhancement of artificial sputum medium. Appl Rheol. 2020;30(1):27–38.
[22] Savin T, Doyle PS. Static and dynamic errors in particle tracking microrheology. Biophys J. 2005;88:623–38.
[23] Puy C, Tucker EI, Wong ZC, Gailani D, Smith SA, Choi SH, et al. Factor XII promotes blood coagulation independent of factor XI in the presence of long-chain polyphosphates. J Thrombosis Haemostasis. 2013;11(7):1341–52.
[24] Martin BRC. Statistics for physicists. London, UK: Academic Press; 1971.
[25] Winter HH, Chambon F. Analysis of linear viscoelasticity of a crosslinking polymer at the gel point. J Rheol. 1986;30(2):367–82.
[26] Winter HH, Mours M. Rheology of polymers near liquid-solid transitions. In: Neutron spin echo spectroscopy viscoelasticity rheology. Berlin, Heidelberg: Springer; 1997. p. 165–234.
[27] Schultz KM, Baldwin AD, Kiick KL, Furst EM. Gelation of covalently cross-linked PEG-heparin hydrogels. Macromolecules. 2009;42(14):5310–6.
[28] Lusignan CP, Mourey TH, Wilson JC, Colby RH. Viscoelasticity of randomly branched polymers in the critical percolation class. Phys Rev E. 1995;52(6):6271.
[29] Martin JE, Adolf D, Wilcoxon JP. Viscoelasticity of near-critical gels. Phys Rev Lett. 1988;61(22):2620.
[30] Savin T, Doyle PS. Electrostatically tuned rate of peptide self-assembly resolved by multiple particle tracking. Soft Matter. 2007;3(9):1194–202.
[31] Tillman BF, Gruber A, McCarty OJ, Gailani D. Plasma contact factors as therapeutic targets. Blood Rev. 2018;32(6):433–48.
[32] Sylman JL, Daalkhaijav U, Zhang Y, Gray EM, Farhang PA, Chu TT, et al. Differential roles for the coagulation factors XI and XII in regulating the physical biology of fibrin. Ann Biomed Eng. 2017;45(5):1328–40.